

Submitted to the Astrophysical Journal

Line Emission from Cooling Accretion Flows in the Nucleus of M 31

Sin ing Liu

Department of Physics, The University of Arizona, Tucson, A Z 85721

Michael J. From erth¹

Department of Physics, The University of Arizona, Tucson, A Z 85721

and

Fulvio M elia²

Department of Physics and Steward Observatory, The University of Arizona, Tucson, A Z 85721

Received _____; accepted _____

¹NSF Graduate Fellow .

²Sir Thomas Lyle Fellow and Megunyah Fellow .

A B S T R A C T

The recent Chandra X-ray observations of the nucleus of M 31, combined with earlier VLA radio and HST UV spectral measurements, provide the strictest constraints thus far available on the nature of accretion onto the supermassive black hole (called M 31* hereafter) in this region. One of the two newly-detected sources within roughly an arcsec of M 31* may be its X-ray counterpart. If not, the X-ray flux from the nucleus must be even lower than inferred previously. Some uncertainty remains regarding the origin of the UV excess from the compact component known as P 2. In our earlier analysis, we developed a unified picture for the broadband spectrum of this source and concluded that M 31* could be understood on the basis of the accretion model for Sgr A* at the Galactic center, though with several crucial differences. Contrary to the 'standard' picture in which the infalling plasma attains temperatures in excess of 10^{10} K near the event horizon, the best fit model for M 31*, under the assumption that the UV radiation is in fact produced by this source, appears to correspond to a cool branch solution, arising from strong line cooling inside the capture radius. Starting its infall with a temperature of about 10^6 K in the post-shock region, the plasma cools down efficiently to about 10^4 K toward smaller radii. An important prediction of this model is the appearance of a prominent UV spike from hydrogen line emission, which for simplicity was handled only crudely in the earlier work. It is our purpose here to model this line emission with significantly greater accuracy, using the algorithm CLOUDY, and to correctly take into account the attenuation along the line of sight. We show that this level of sophistication reproduces the currently available multi-wavelength observations very well. Very importantly, we predict a spectrum with several additional prominent emission lines that can be used to verify the model with future high-resolution observations. A non-detection of the predicted line emission from M 31* would then tilt the favored accretion picture in the direction of a hot Sgr A*-type of model, though with only a single point remaining in the spectrum of M 31*,

{ 3 {

additional observations at other wavelengths would be required to seriously constrain this system .

Subject headings: accretion | black hole physics | Galaxy: center | galaxies: individual
(M 31) | galaxies: nuclei | X-rays: galaxies

1. INTRODUCTION

The nucleus of M 31 contains two components, P 1 & P 2, separated by about 0.5 ± 1.9 pc (Lauer et al. 1993). Its optical image is dominated by P 1 while there is a UV upturn in P 2 (King et al. 1995). The kinematics of stars near the nucleus (Kormendy & Bender 1999) suggests that P 1 & P 2 may be identified as the turning points of an elliptical distribution of stars orbiting the central black hole of mass $3.0 \pm 10^7 M_\odot$ in a slightly eccentric orbit (Tremaine 1995). However, the relatively intense UV emission from P 2 remains a puzzle.

Based on earlier radio observations of M 31* (Crane, Dickel, & Cowan 1992), Melia (1992) suggested that its nature may be similar to that of the supermassive black hole, Sgr A*, at the Galactic center. Identifying the X-ray object TF56 (Trinchieri & Fabbiano 1991) with M 31*, King et al. (1995) proposed a compact nonthermal source at this location. However, subsequent high resolution HST observations have partially resolved P 2 (Lauer et al. 1998; Brown et al. 1998), showing that it has a halfpower radius of $0.06''$. Lauer et al. (1998) argued that these new observations point to the UV upturn as being produced by a tightly bound cluster of early type stars. Even so, this picture does not appear to be complete.

The apparent identification of an X-ray source with M 31* (Garcia et al. 2000) suggested that the accretion process in M 31* and Sgr A* must be quite different (Liu & Melia 2001). If neither of the two sources detected within about an arcsecond of M 31* are its counterpart, this would place a strict upper limit on its X-ray flux and hence the temperature of the emitting gas. In this picture, the UV radiation is an extension of M 31*'s radio component, which, however, must turn over below ~ 1 keV.

Instead of the model for Sgr A* in which the accreting plasma reaches temperatures of 10^{10} K or higher (e.g., Shapiro 1973a; Melia 1992, 1994), M 31* appears to correspond well to a second branch of solutions in which cooling dominates heating and the gas settles down to a much lower temperature during its infall. An optically thin plasma with a temperature of about $10^5 \pm 10^7$ K, a typical value at the capture radius $r_c = 2GM/\sqrt{1}$ of a supermassive black hole accreting from

stellar winds (Coker & Melia 2000), lies on the unstable portion of the cooling curve (Gehrels & Williams 1993). Here, v_1 is the velocity of the ambient gas flowing past the central black hole. Liu & Melia (2001) showed that in this case two branches of solutions exist, distinguished by the relative importance of cooling versus compressional heating at r_c . Depending on the initial temperature $T(r_c)$ and the mass accretion rate \dot{M} , the plasma either settles onto a hot branch or a cool branch, characterized by temperatures of 10^{10} K and 10^4 K, respectively, toward smaller radii.

Comparing these two solutions to the observations, Liu & Melia (2001) argued that M 31* must lie on the cool branch, and that we should therefore see a spectral signature of its cooling flow, particularly a prominent UV spike due to hydrogen line emission and soft X-ray line recombination. The purpose of this paper is to present a significantly more detailed calculation of the broadband emission spectrum, correcting also for the attenuation along the line of sight. In section 2, we discuss the standard Bondi-Hoyle model for supermassive black holes accreting from the ambient medium. In section 3 & 4, we discuss the specific details of our line emission calculations and we identify several emission lines that may be used to verify our model. Section 5 presents the conclusions.

2. LOW ANGULAR MOMENTUM ACCRETION FLOW

In this section, we briefly summarize the Bondi-Hoyle accretion model for a low luminosity accreting supermassive black hole embedded within a gaseous environment. The latter may be produced by the winds of nearby stars. Gas flowing past the black hole will be captured at a rate determined by its velocity and specific angular momentum relative to the compact object. Because winds far from the stars are always highly supersonic, many shocks can form where the winds collide before the gas is captured within the central gravitational field. These shocks dissipate most of the kinetic energy and heat the plasma to a temperature of $(3\mu/4)^2 = 3R_g$, where R_g is the gas constant and μ is the molecular weight per particle, which is about 1=2 for a fully ionized plasma. During the infall, the plasma accelerates under the influence of gravity and

again goes transonic. We base our analysis on the global structure inferred for these flows from existing 3D hydrodynamical simulations of the infalling gas (e.g., Coker & Melia 1997), and we take our starting point to be a radius where the plasma has already re-crossed into the supersonic region. Our analysis will adopt a purely radial flow, for which consistency requires a negligibly small specific angular momentum in the accreting gas.

Due to their low luminosity, supermassive black holes accreting in this fashion can be treated with significant simplification. For example, the energy loss due to radiation can be treated with just a cooling term in the energy equation and the related effect on the dynamics of the flow is negligible. In this sense, the structure of the accretion flow and the radiation may be handled separately.

2.1. Dynamical Equations

The stress-energy tensor for a radial accretion flow with a frozen-in magnetic field is given by (Novikov & Thorne, 1973):

$$T_{\alpha\beta} = \rho u_\alpha u_\beta + p(g_{\alpha\beta} + u_\alpha u_\beta) + \frac{1}{8}(2B^2 u_\alpha u_\beta + B^2 g_{\alpha\beta} - 2B_\alpha B_\beta); \quad (1)$$

where $\rho = n k_B T = 2 + n m_p c^2$ is the energy density. The general expression for ρ is given by Chandrasekhar (1939):

$$\rho = x \frac{3K_3(x) + K_1(x)}{4K_2(x)} - 1 + y \frac{3K_3(y) + K_1(y)}{4K_2(y)} - 1; \quad (2)$$

where $x = m_e c^2 / k_B T$, $y = m_p c^2 / k_B T$ and K_i is the i th order modified Bessel function. Also, n is the baryon number density, and $p = n k_B T$ is the gas pressure. The other symbols have their usual meaning. The shear and bulk viscosity has been neglected in the equation because the flow is spherically symmetric. In the case that the radiation is not very strong, the radiation can be treated as an external field, which just contributes a cooling term to the accretion flow. So we don't include it in the stress-energy tensor either.

In Schwarzschild coordinates, the metric is given as

$$ds^2 = -c^2 dt^2 = -\left(1 - \frac{2GM}{r c^2}\right) c^2 dt^2 + \frac{1}{1 - \frac{2GM}{r c^2}} dr^2 + r^2 (d\theta^2 + \sin^2 \theta d\phi^2) ; \quad (3)$$

where M is the mass of the supermassive black hole. Then we have $u = (u^t; u^r; 0; 0) = (dt/d\tau; dr/cd\tau; 0; 0)$, which is dimensionless in our notation. Because the magnetic field in a spherical accretion flow is dominated by its radial component (Shapiro 1973b), one has $B = (B^t; B^r; 0; 0)$. The electric field is always zero in the comoving frame of a fully ionized plasma with frozen-in magnetic field, so B is orthogonal to u :

$$B_\mu u^\mu = 0 ; \quad (4)$$

The dynamical equations for the radial accretion flow are as follows:

$$(nu)_{;\mu} = 0 ; \quad (5)$$

$$T_{;\mu} = -F_{;\mu} ; \quad (6)$$

where $F_{;\mu} = T_{\text{rad};\mu}$ is the divergence of the energy-momentum tensor T_{rad} for the photons, which gives the plasma's energy and momentum loss rate due to radiation. The cooling rate in the comoving frame of the flow is given by $\dot{Q} = cF_\mu u^\mu$.

For a steady flow, the continuity Equation (5) gives

$$\dot{M} = 4\pi r^2 c u^r n_p ; \quad (7)$$

where the accretion rate \dot{M} is a constant.

The law of local energy conservation is given by projecting Equation (6) onto u , for which

$$c u^\mu T_{\mu;\nu} = -\dot{Q} u_\nu ; \quad (8)$$

that is,

$$\frac{d}{d\tau} \left(\frac{1}{n} \right) = -\frac{c}{u^r} \frac{1}{n} + \frac{\dot{Q}}{n} ; \quad (9)$$

where

$$\dot{Q} = c u^\mu T_{\text{mag}\mu\nu} u^\nu ; \quad \dot{Q} = \frac{c}{4\pi r} (2B^2 u_r + r u_r B^0 B^0) \quad (10)$$

is the heating term due to the annihilation of the magnetic field. As usual, we will use prime to denote a derivative with respect to r and an over-dot to denote a derivative with respect to t . $T_{mag} = (2B^2 u u + B^2 g - 2B B) = 8$ is the Maxwell stress-energy associated with the frozen-in magnetic field.

The Euler equations are given by

$$(g + u u) T_{,r} = F + \frac{u}{c} : \quad (11)$$

Only the radial component of the equation is non-trivial. It gives

$$(p +) u_r^r u = (g + u^r u) p_{,r} ; \quad (12)$$

where we have neglected the radiation pressure and magnetic pressure, which are much smaller than the thermal pressure.

Then the equations for the radial velocity and temperature are:

$$\frac{1}{2} \frac{d}{dr} u_r^2 = \frac{p^0}{p +} 1 + u_r^2 - \frac{2GM}{rc^2} - \frac{GM}{r^2 c^2} ; \quad (13)$$

$$\frac{T^0}{T} = \frac{1}{k_B T n c u_r} - \frac{1}{u_r} + \frac{2}{r} : \quad (14)$$

Because the spacetime geometry is dominated by the supermassive black hole, all of these equations ignore the effects of self-gravity within the accreting gas. These equations are readily solved numerically to provide the radial structure of the infalling gas once the boundary conditions and the magnetic field are specified.

2.2. Boundary Conditions and Magnetic Field

In principle, a precise knowledge of the wind sources surrounding the accretor would provide all the necessary conditions at the capture radius to determine the structure of the infalling gas uniquely. However, only some global properties of the ambient medium are known adequately well. For example, at the Galactic center, the average density and flow velocity have been determined

from emission-line measurements, but even there, a lack of information on the de-projected distance along the line of sight to the accretor prevents us from positioning the sources with certainty around the black hole. The ambient conditions in the much more distant nucleus of M 31 are even more difficult to identify with precision. Our approach will instead be to use the accurately known spectrum produced by the accreting gas to guide our selection of the boundary conditions, which therefore become adjustable parameters for the fit.

Taking our cue from the conditions prevalent at the Galactic center, we adopt a wind velocity v_1 of about 500 km s^{-1} , which then also determines the downstream plasma temperature for a strong shock:

$$T = (3 v_1^2 / 4) = 3 R_g : \quad (15)$$

Typically, $T \approx 3 \times 10^6 \text{ K}$. Three-dimensional hydrodynamic simulations show that the region between the shocks and the transonic point is more or less isothermal. So we would expect the temperature at the outer boundary of our modeled region to be about several million degrees Kelvin.

HST observations (Lauer et al. 1998) show that the extended UV source in P 2 has a radius of about 0.2 pc ($\approx 10^5 r_s$, where $r_s = 2GM/c^2$ is the Schwarzschild radius of the central black hole). The outer boundary should have roughly the same scale as this. To ensure that this outer boundary is located below the transonic point (since we are limiting our domain of solution to this region | see above), the radial velocity of the flow must be larger than its thermal velocity at that point. We have already limited the temperature at the outer boundary. This therefore provides a lower limit for the radial velocity. At the same time, the flow must be bounded, so its radial velocity cannot exceed the free fall value at this radius.

With M and u_r known, the accretion rate then depends on the ambient gas density. Although Ciardullo et al. (1998) have argued that the ionized gas density in the nucleus of M 31 changes dramatically, dropping from $> 10^4 \text{ electrons cm}^{-3}$ at a radius of $7''$ or 23 pc to $10^2 \text{ electrons cm}^{-3}$ at $1''$ or 200 pc , the actual density near the capture radius may still be quite different from this given the differences in length scales. As such, the accretion rate, or the gas density at

the outer boundary, remain as adjustable parameters.

The structure and intensity of the magnetic field are also poorly known in this context, given the uncertain nature of magnetic field dissipation within a converging flow. Following the assessments of Kowalenko & Melia (1999), and their application to Sgr A* in the outer region of the accretion flow (Coker & Melia 1997), we will invoke a sub-equipartition field compared to the thermal energy density. That is, we will take $B^2/8\pi = \beta n k_B T/2$, where $\beta < 1$.

2.3. Dichotomy of the Accretion Profiles

Figure 1 shows the cooling curve for an optically thin plasma with cosmic abundances. The thin solid curve is that given by Gehrels & Williams (1993), which we used in our previous calculation. The thick solid curve gives a more accurate cooling curve based on more detailed modeling with CLOUDY (Ferland 1996). This is the curve used for the calculations reported in this paper. It is evident that the plasma is located in an unstable portion of this curve when its temperature lies between 10^5 and 10^7 K. As we have seen above, the temperature downstream of the capture radius is typically several million Kelvin. Thus, depending on the gas density in this region, which determines the cooling rate at the outer boundary and the accretion rate for a given radial velocity, the plasma may either heat up to about 10^{10} K, or cool down to around 10^4 K.

Figure 2 illustrates this dichotomy. The thick solid curve corresponds to our best fit model for the multi-wavelength observations of M 31*, which has an outer boundary r_o of $10^5 r_s$ (008), a radial velocity of one half of the free fall velocity, an accretion rate of $1.5 \times 10^{25} \text{ g s}^{-1}$ and a magnetic parameter $\beta = 0.003$. The outer boundary temperature is given by the ratio of the thermal to gravitational energy density, which is 0.068 for the best fit model. To emphasize the accretion rate dependence of the solutions, we also show in this figure the temperature profiles for two configurations with different accretion rates, which are $1.5 \times 10^{24} \text{ g s}^{-1}$ and $1.5 \times 10^{23} \text{ g s}^{-1}$ for the dashed curve and the thin solid curve, respectively. Clearly, the solutions depend rather sensitively on the accretion rate. We will return to this point in section 5 below. It appears that

in order for M 31* to simultaneously account for both the radio and UV spectral components, the post-shock gas initiating its infall toward the central accretor is highly unstable to cooling. For this reason, the temperature of the plasma in the best-fit model drops quickly from 10^6 K in the post-shock/capture region to 10^4 K for the remainder of its inward flow.

In the hot branch, the cooling is dominated by thermal bremsstrahlung radiation. We would expect a flat spectrum which cuts off at $\epsilon_{\text{ph}} T = h$. Figure 3 shows the spectra corresponding to the three configurations in Figure 2. In this figure, the two more constraining optical upper limits are from Lauer et al. (1998) and the three near Infrared upper limits are from Corbin et al (2001). The other data are discussed in Liu & Melia (2001). Note that these spectra do not include the contribution from cyclo-synchrotron emission, which is absent in the cool branch solutions, but would produce an additional peak at radio frequencies for the hot branch profiles. The magnitude and location of this cyclo-synchrotron peak would depend on the strength of the magnetic field. Clearly, the Chandra X-ray upper limit (or detection, depending on whether or not one of the sources near M 31* is its counterpart) already rules out the hot branch solution for M 31*, under the assumption that the radio component extends into the UV region, even without the additional problems introduced at radio wavelengths by this additional component. The cool branch solution, on the other hand, accounts very well for the radio and UV emission, and it features strong line emission due to the dominant line cooling component in the cooling function. Even so, the configuration with the low accretion rate can't produce the observed radio and UV flux, so there is a restricted range of parameter values at the outer boundary that appear to be consistent with the data.

3. CALCULATING THE EMISSION SPECTRUM

The emission spectrum of a cooling gas is a function of the density n and temperature T , which in turn are both functions of radius. With the assumption of spherical symmetry, the mean

emissivity (in units of energy per unit time per unit volume per unit frequency interval) is

$$j(r; \nu) = j^{\text{brem}}(n(r); T(r)) + \sum_{\text{lines}} j^{\text{line}}(n(r); T(r)) \delta(\nu - \nu_{\text{line}}(r)); \quad (16)$$

where

$$\nu_{\text{line}}(r) = \frac{\nu_{\text{line}}^0 \frac{1}{\sqrt{1 - v(r)^2/c^2}}}{(1 + v(r) \cos \theta/c)} \quad (17)$$

is the special relativistic correction to the monochromatic flux of moving emitters (Corbin

1997); $j^{\text{brem}}(n; T) \approx 6.8 \times 10^{38} n^2 T^{1/2} \exp(-h/kT) \text{ erg s}^{-1} \text{ cm}^{-3} \text{ Hz}^{-1}$ is the mean

emissivity due to thermal bremsstrahlung (Frank, King, & Raine 1992), with the ionization

fraction $x = (1.0 + 0.445 T^{-1} e^{157890/T})^{-1}$ obtained following the prescription given in Rossi et al.

(1997); $j^{\text{line}}(n; T)$ is the mean emissivity (in units of energy per unit time per unit volume) due to line emission; and

$$\nu_{\text{line}}(r) = \nu_{\text{line}}^0 \frac{1}{\sqrt{1 - v(r)^2/c^2}} \quad (18)$$

is the Doppler-corrected line frequency, with ν_{line}^0 being the rest-frame line frequency. General

relativistic effects have been ignored as the vast majority of emission occurs at radii $r \ll R$.

Computationally, we view the inflow as a series of concentric spherical shells, each of which is characterized by a set of physical parameters. The velocity $v(r)$ and density $n(r)$ are specified by the equations of continuity and motion, and the temperature $T(r)$ is specified by the energy balance equation, including terms for line and bremsstrahlung cooling (Gehrels & Williams 1993).

The central mass is assumed to be $M = 3 \times 10^7 M_\odot$ and the mass accretion rate is set at $\dot{M} = 1.5 \times 10^{25} \text{ g s}^{-1}$, corresponding to the best fit model temperature profile shown in Figure 2.

We model each shell as a coronal equilibrium zone (appropriate for gas which is mainly collisionally ionized) and use the photoionization code CLOUDY (Ferland 1996; CLOUDY 94.00) to compute the line emissivities. Cosmic abundances are assumed throughout, with no grains present due to the high temperatures. Radiative transfer effects between the zones are neglected, as gas is optically thin above 0.1 GHz.

To obtain a spectrum of the flux density, the emissivity is integrated over the entire inflow

volume:

$$F = \frac{1}{4 D_{M31}^2} \int_0^Z r^2 \sin \theta dr d\theta d\phi ; \quad (19)$$

where $D_{M31} = 784$ kpc is the distance to M 31 (Stanek & G amavich 1998). The flux density is then corrected for extinction along the line of sight due to absorption (Cruddace et al. 1974; Morrison & McCammon 1983) and reddening (Cardelli, Clayton, & Mathis 1989), assuming a column depth of $N_H = 2.8 \times 10^{21} \text{ cm}^{-2}$ based on Chandra observations (Garcia et al. 2000), cosmic elemental abundances (Dalgarno & Layzer 1987), $A_V = 0.24$ (Lauer et al. 1993), and $E(B - V) = 0.11$ (King, Stanford, & Crane 1995).

4. RESULTS

Figure 4 shows the intrinsic flux spectrum calculated with our model. The spectrum (and cooling) is dominated by the UV recombination lines of warm Fe, O, Si, and S species present in the outer flow region.

Figure 5 shows the model spectrum corrected for extinction. It is evident that the strongest emission lines are effectively extinguished by the intervening column of gas. The surviving optical-UV and soft X-ray components both show very strong line emission superimposed on a bremsstrahlung continuum, and should be easy to distinguish from, e.g., the composite spectrum of a stellar population. For comparison, the spectra of $T = 10,000$ K and $T = 30,000$ K stars computed from Atlas stellar atmosphere modeling (Kurucz 1991) are also presented in the figure.

An expanded view of the modeled UV and X-ray spectra are shown in Figures 6 and 7. High spatial resolution observations of M 31* at these wavelengths may provide a very straight-forward test of this cooling accretion flow picture. In particular, the UV spectrum is characterized by very strong line emission; Table 1 lists the intensities of the strongest emission lines relative to Ly γ .

5. DISCUSSION

As mentioned in section 2.3, these solutions are rather sensitive to the outer boundary conditions, particularly the accretion rate. For these simulations, we have used a simplified scheme in which compressional and magnetic heating balance line cooling in the outer region. In reality, turbulent heating may also play an important role in stabilizing the temperature. Additional heating may be provided by the disturbance generated by the stellar population around P2. In any event, the essential feature of this model is that regardless of what happens at large radii, line cooling can dominate over the heating processes at small radii when the accretion rate is large enough. This inner cool region is important because the observed weak radio emission does not allow the plasma to be heated up. The two radio measurements of M 31* give a flux density of $28 - 39 \text{ Jy}$ at 3.6 cm (Crane et al. 1992 & 1993). The 3.6 cm radio flux from an optically thick spherical emitter can be estimated using the following equation:

$$\begin{aligned} F(3.6 \text{ cm}) &= \frac{r_s}{D_{M31}} \frac{R}{r_s} \frac{2}{2} \frac{k_b T}{2} \\ &= 0.895 \frac{T}{10^{10} \text{ K}} \frac{R}{r_s} \frac{2}{2} \text{ Jy} : \end{aligned} \quad (20)$$

Thus, a source with radius $10 r_s$ and a temperature of several times 10^{10} K will produce far too much flux at 3.6 cm . On the other hand, a hot optically thin source cannot produce the strong UV emission via self Comptonization of the radio photons. If the UV component is in fact associated with M 31*, this argument also rules out many other models developed in recent years to account for the emissivity of supermassive black holes in the cores of nearby galaxies, including Sgr A* at the Galactic center (the ADAF model, Narayan, Yi, & Mahadevan 1995; the ADIOS model, Blanford & Begelman 1999; and the jet model, Falcke & Marko 2000). However, if the UV emission is not associated with M 31*, a hot optically thin plasma may still account for the radio emission, as it does for Sgr A*. Distinguishing between these two scenarios via the observation of UV lines in M 31*'s spectrum makes our proposed measurements highly desirable.

In calculating the spectrum for the hot branch solution in Figure 3, we have not included the effects due to a magnetic dynamo, should the gas circularize before it reaches the event horizon.

In the case of Sgr A *, the dominant contribution to the mm and sub-mm spectrum is made by a Keplerian structure within the inner $5 r_S$ or so (Melia, Liu & Coker 2000, 2001). In the case of M 31*, this region may or may not exist, depending on how much specific angular momentum is carried inward. For the same conditions as in Sgr A *, M 31* would not have a Keplerian region since $r_S(M 31) \approx 10 r_S(\text{Sgr A})$, i.e., the gas would not circularize before crossing the event horizon. So the model for Sgr A * may not work here. The much larger accretion rate implied by our model also rules out the possibility of a standard optically thick disk being present in M 31*. As shown in Figure 8, even with an accretion rate more than 6 orders of magnitude smaller than the accretion rate we infer for the best fit case, a small optically thick disk still produces too much optical radiation compared to the observations. Such an optically thick disk would not be able to account for the UV upturn either, making it unlikely that such a structure is present in the nucleus of M 31.

In Figures 3 and 8, we have treated the Chandra flux measurements of the two nearest X-ray sources to M 31* as upper limits, since neither of these has been established with confidence as the actual counterpart to the radio source. A slightly different fit, assuming that the so-called "southern" source is indeed the counterpart, was presented in Liu & Melia (2001). None of the conclusions presented in this paper are affected qualitatively in this instance, except for slight differences in the recombination line intensities. However, if the "northern" source turns out to be the actual counterpart (see Garcia et al. 2000), the cold accretion model will not work for M 31*. A close inspection of Figure 8 shows that the X-ray spectrum (indicated by the butterfly) is then too hard to be described adequately by bremsstrahlung emission. The nature of M 31* is therefore still rather uncertain, making further study of this very interesting object highly desirable.

6. ACKNOWLEDGMENTS

This work was supported by an NSF Graduate Fellowship and by NASA grants NAG 5-8239 and NAG 5-9205 at the University of Arizona, and by a Sir Thomas Lyle Fellowship and a Megunyah Fellowship for distinguished overseas visitors at the University of Melbourne.

R E F E R E N C E S

- Blandford, R. D. & Begelman, M. C. 1999, *MNRAS*, 303, L1
- Brown, T. M., Ferguson, H. C., Stanford, S. A. & Deharveng, J.-M. 1998, *ApJ*, 504, 113
- Cardelli, J. A., Clayton, G. C., & Mathis, J. S. 1989, *ApJ*, 345, 245
- Chandrasekhar, S. 1939. *An Introduction to the Study of Stellar Structure* (New York: Dover)
- Ciardiullo, R., Rubin, V. C., Jacoby, G. H., Ford, H. C. & Ford, W. K. Jr. 1988, *AJ*, 95, 438
- Coker, R. F. & Melia, F. 1997, *ApJ Letters*, 488, L149
- Coker, R. F. & Melia, F. 2000, *ApJ*, 534, 723
- Corbin, M. R. 1997, *ApJ*, 485, 517
- Corbin, M. R., O'Neil, E. & Reike, M. J. 2001, *AJ*, submitted
- Crane, P. C., Dickel, J. R. & Cowan, J. J. 1992, *ApJ Letters*, 390, L9
- Crane, P. C., Cowan, J. J., Dickel, J. R. & Roberts, D. A. 1993, *ApJ Letters*, 417, L61
- Cruddace, R., Paresce, F., Bowyer, S., & Lampton, M. 1974, *ApJ*, 187, 497
- Dalgarno, A., & Layzer, D. 1987, *Spectroscopy of Astrophysical Plasmas* (Cambridge: Cambridge University Press)
- Falcke, H. & Marko, S. 2000, *A & A*, 362, 113
- Ferland, G. J. 1996, *Hazy, a brief introduction to CLOUDY 94.00*
- Frank, J., King, A., & Raine, D. 1992, *Accretion Power in Astrophysics* (Cambridge: Cambridge University Press)
- Garcia, M. R., Murray, S. S., Primini, F. A., Forman, W. R., Jones, C., McClintock, J. E., & Jones, C. 2000, *ApJ*, 537, L23

Garcia, M. R., Murray, S. S., Prini, F. A., Forman, W. R., Jones, C., & McClintock, J. E. 2001, *IAU 205, Galaxies at the Highest Angular Resolution*, eds. Schilizzi, Vogel, Paresce, & Elvis, in press.

Garcia, M. R., 2001, private communication.

Gehrels, N. & Williams, E. D. 1993, *ApJ*, 418, L25

King, I. R., Stanford, S. A., & Crane, P. 1995, *AJ*, 109, 164

Komendy, J. & Bender, R. 1999, *ApJ*, 522, 772

Kowalenko, V. & Melia, F. 1999, *MNRAS*, 310, 1053

Kunucz, R. L. 1991, *Proceedings of the Workshop on Precision Photometry: Astrophysics of the Galaxy*, eds. Davis, Philip, Uppgren, & James (Davis: Schenectady)

Lauer, T. R., et al. 1993, *AJ*, 106, 1436

Lauer, T. R., Faber, S. M., Athar, E. A., Grillmair, C. J., & Scowen, P. A. 1998, *AJ*, 116, 2263

Liu, S. & Melia, F. 2001, *ApJ Letters*, 550, L151

Melia, F. 1992, *ApJ Letters*, 398, L95

Melia, F. 1994, *ApJ*, 426 577

Melia, F., Liu, S., & Coker, R. F. 2001, *ApJ*, in press

Melia, F., Liu, S., & Coker, R. F. 2000, *ApJ Letters*, 545, L117

Morrison, R., & McMahon, D. 1983, *ApJ*, 270, 119

Narayan, R., Yi, I., & Mahadevan, R. 1995, *Nature*, 374, 623

Novikov, I. D. & Thorne, K. S. 1973, *Black Holes* (edited by C. Dewitt & B. S. Dewitt, Gordon and Breach Science Publishers)

Rossi, P., Bodo, G., Massaglia, S., & Ferrari, A. 1997, *AA*, 321, 672

Shapiro, S. L. 1973a, *ApJ*, 180, 531

Shapiro, S. L. 1973b, *ApJ*, 185, 69

Stanek, K. Z. & Gammie, P. M. 1998 *ApJ Letters*, 503, L131

Tremaine, S. 1995, *AJ*, 110, 628

Trinchieri, G. & Fabbiano, G. 1991, *ApJ*, 382, 82

Table 1. Attenuated Emission Line Intensities

Line ^y	Intensity ^z
Ly 1216	1.00
O VI 1032;1038	0.59
Mg II 2796;2804	0.47
C IV 1548;1551	0.16
N V 1239;1242	0.13
O IV 1399	0.13
S VI 933;945	0.07
C II 2326	0.06
C III 977	0.06
Ne VI 999	0.06
O V 1215	0.03
Si III 1207	0.03
Si III 1891	0.03
Ly 1026	0.02
Ly 973	0.02
C I 1657	0.02
N III 991	0.02
O III 1661;1666	0.02

^yAll wavelengths in Å.^zRelative to Ly 1216.

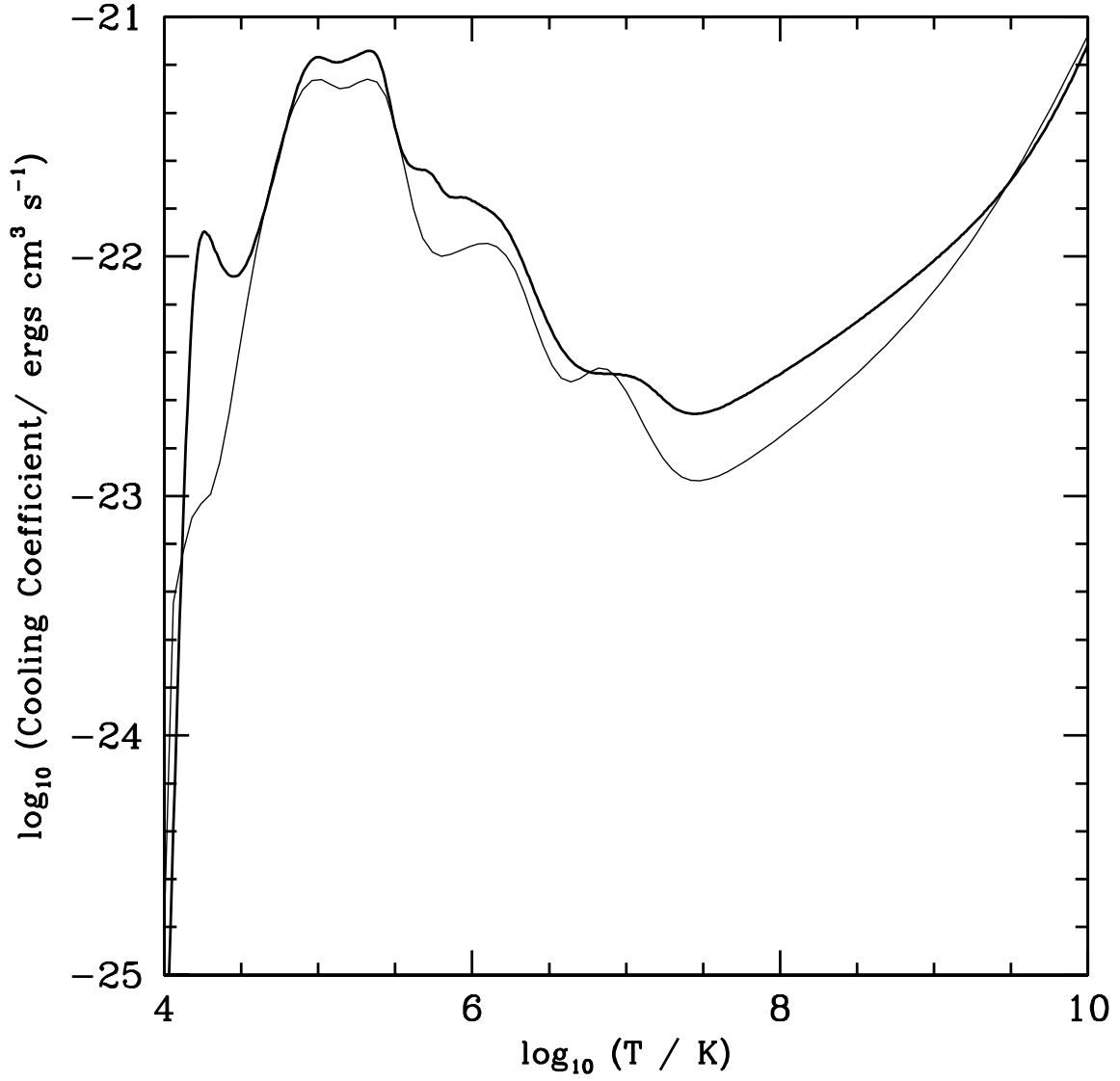


Fig. 1. Temperature dependence of the cooling coefficient, defined to be the cooling rate divided by the baryon number density squared, for an optically thin plasma with cosmic abundances. The thick solid curve is the coefficient used in this paper. The thin solid curve is the result given by Gehrels & Williams (1993), which we used in our previous calculation (Liu & Melia 2001).

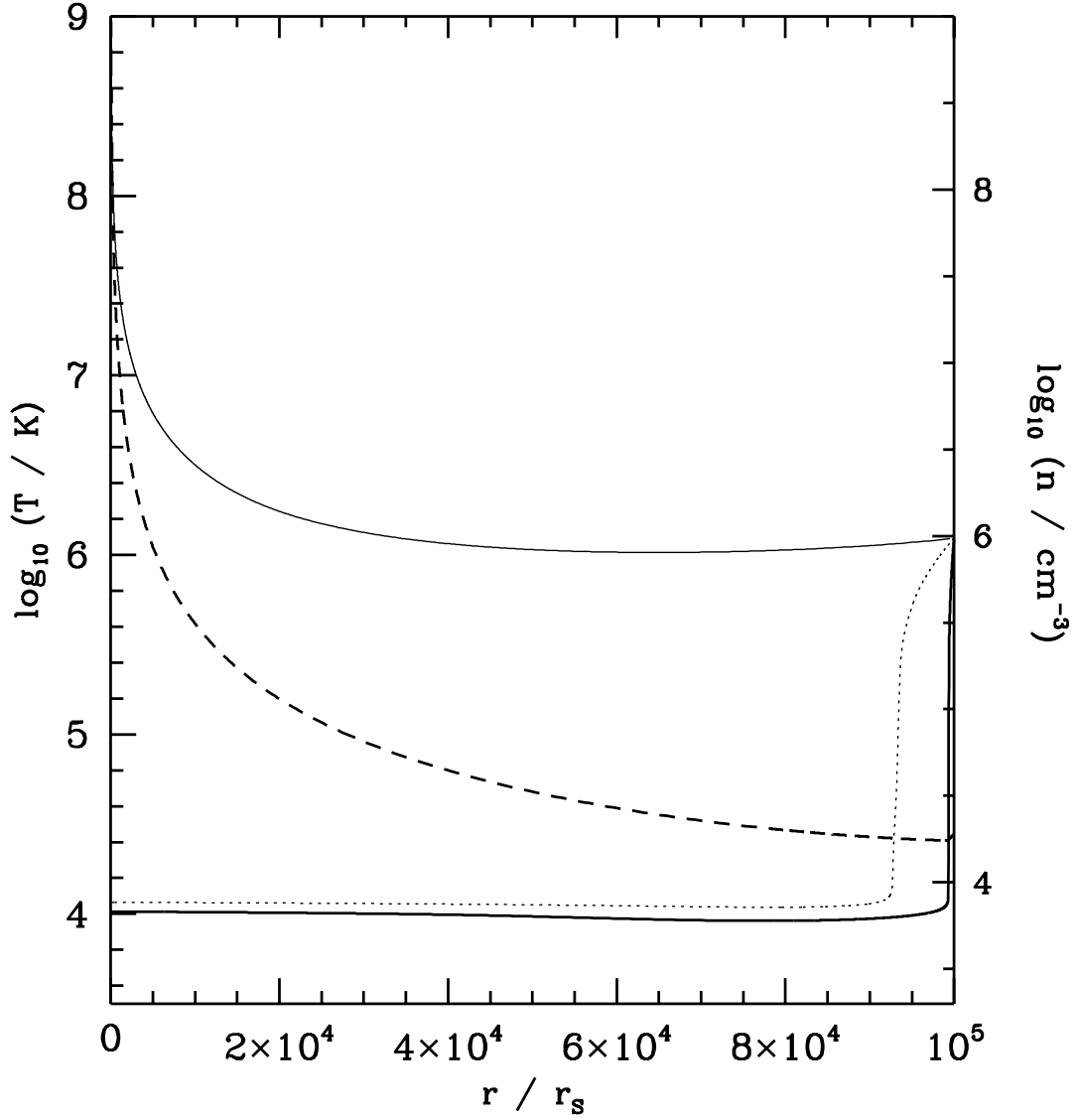


Fig. 2. Temperature profile for the accreting gas, for three values of accretion rate. The initial temperature in all cases is $1.24 \times 10^8 \text{ K}$. The accretion rates are $1.0 \times 10^{23} \text{ g s}^{-1}$ (thin, solid curve | the hot branch solution), $1.0 \times 10^{24} \text{ g s}^{-1}$ (dotted curve) and $1.0 \times 10^{25} \text{ g s}^{-1}$ (thick, solid curve | the best fit model for M 31*). Also shown here is the run of proton density (dashed curve) of the best fit model, whose scale appears on the right hand side.

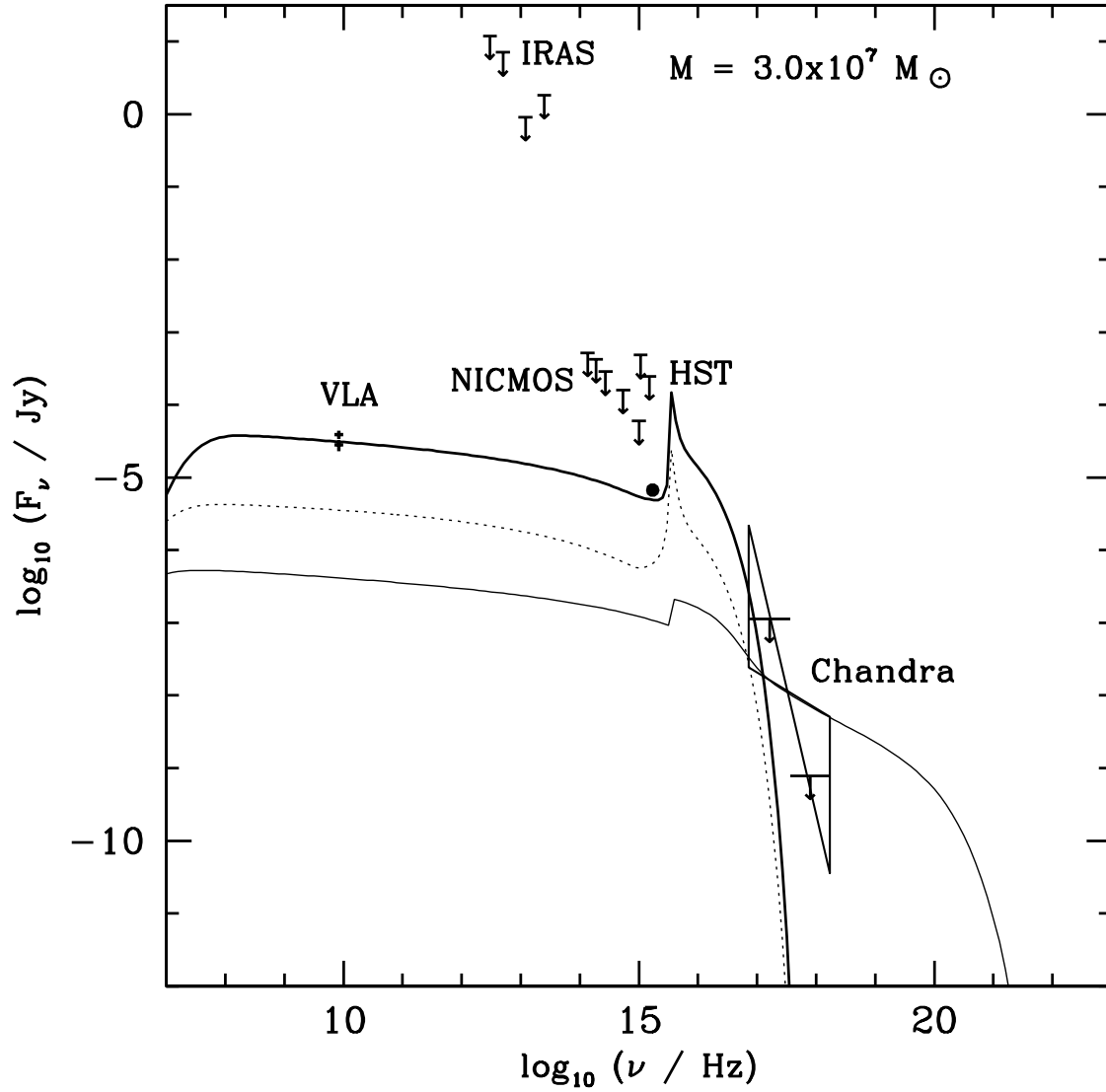


Fig. 3. | A comparison of the overall spectrum arising from each of the three cases depicted in Fig. 2. The line types have the same definitions as those in the figure. The X-ray upper limits correspond to the so-called "southern" source detected near M 31* by Chandra, whereas the butterfly shows the measured spectrum for the "northern" source.

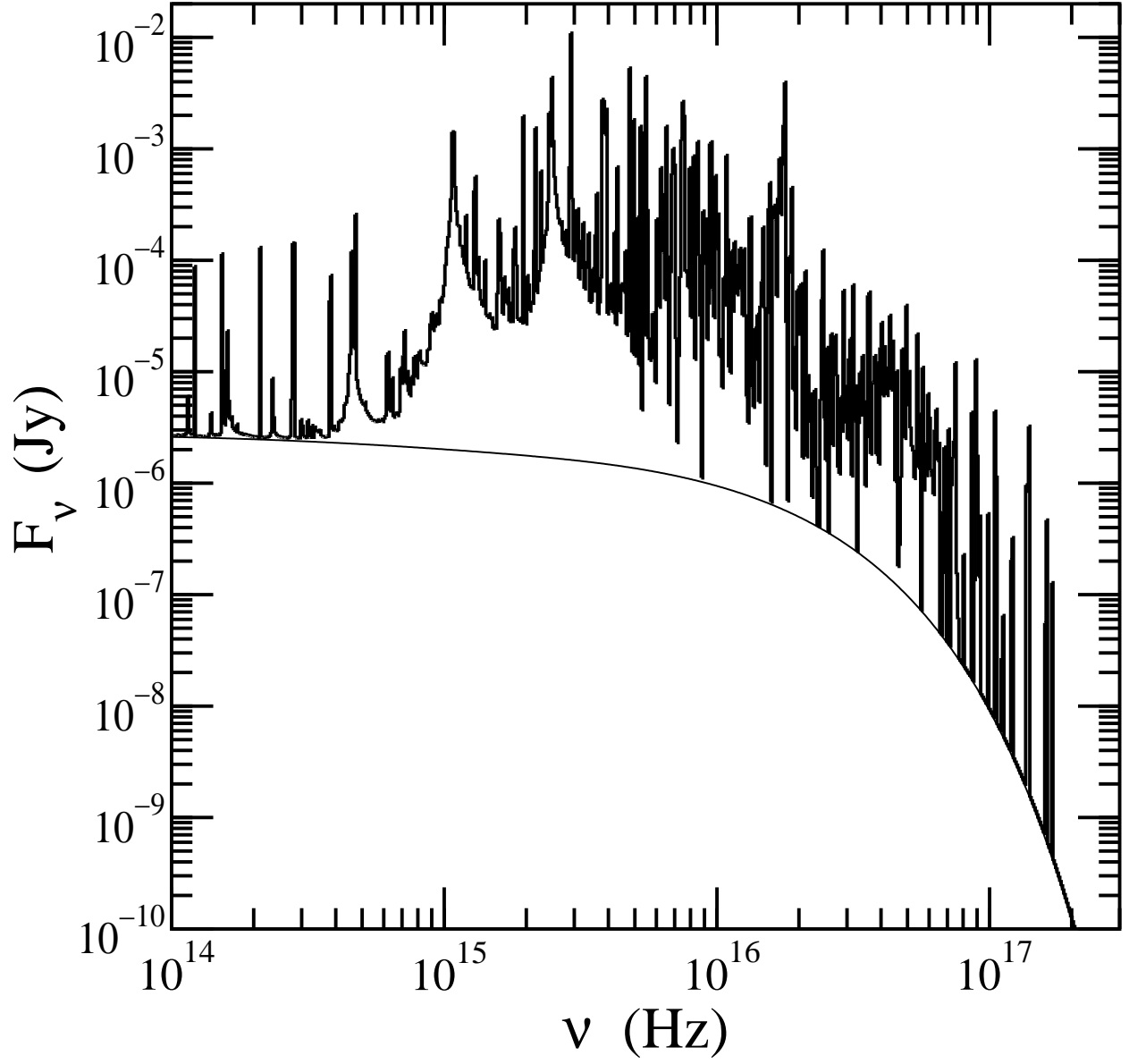


Fig. 4. | Modeled intrinsic bremsstrahlung (thin curve) and bremsstrahlung plus line (dark, heavy curve) spectra.

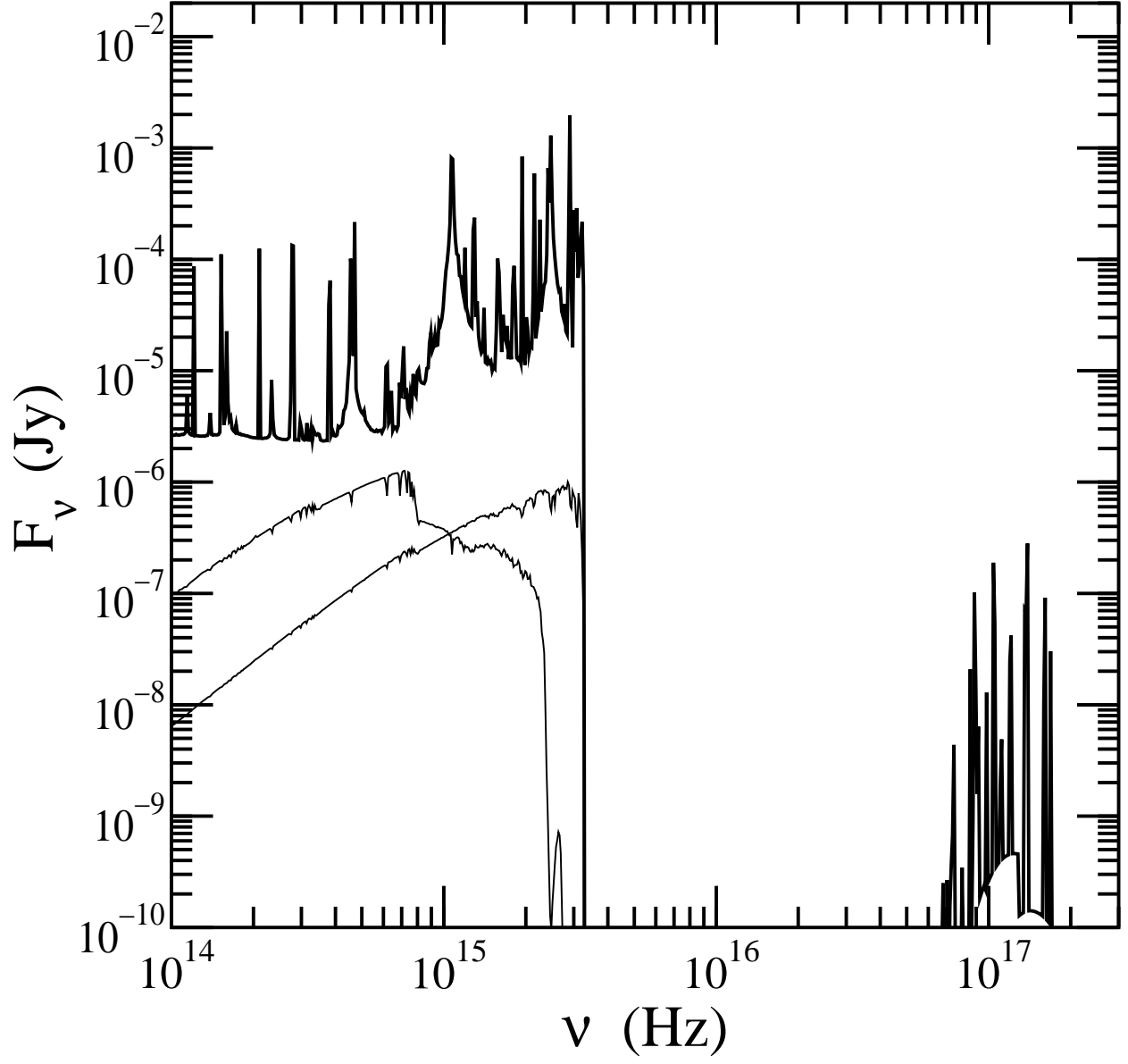


Fig. 5. | Modeled line plus bremsstrahlung spectrum corrected for extinction and reddening (dark). Shown for comparison are stellar atmosphere spectra for $T = 10,000$ K and $T = 30,000$ K stars (thin curves), arbitrarily scaled. See text for description.

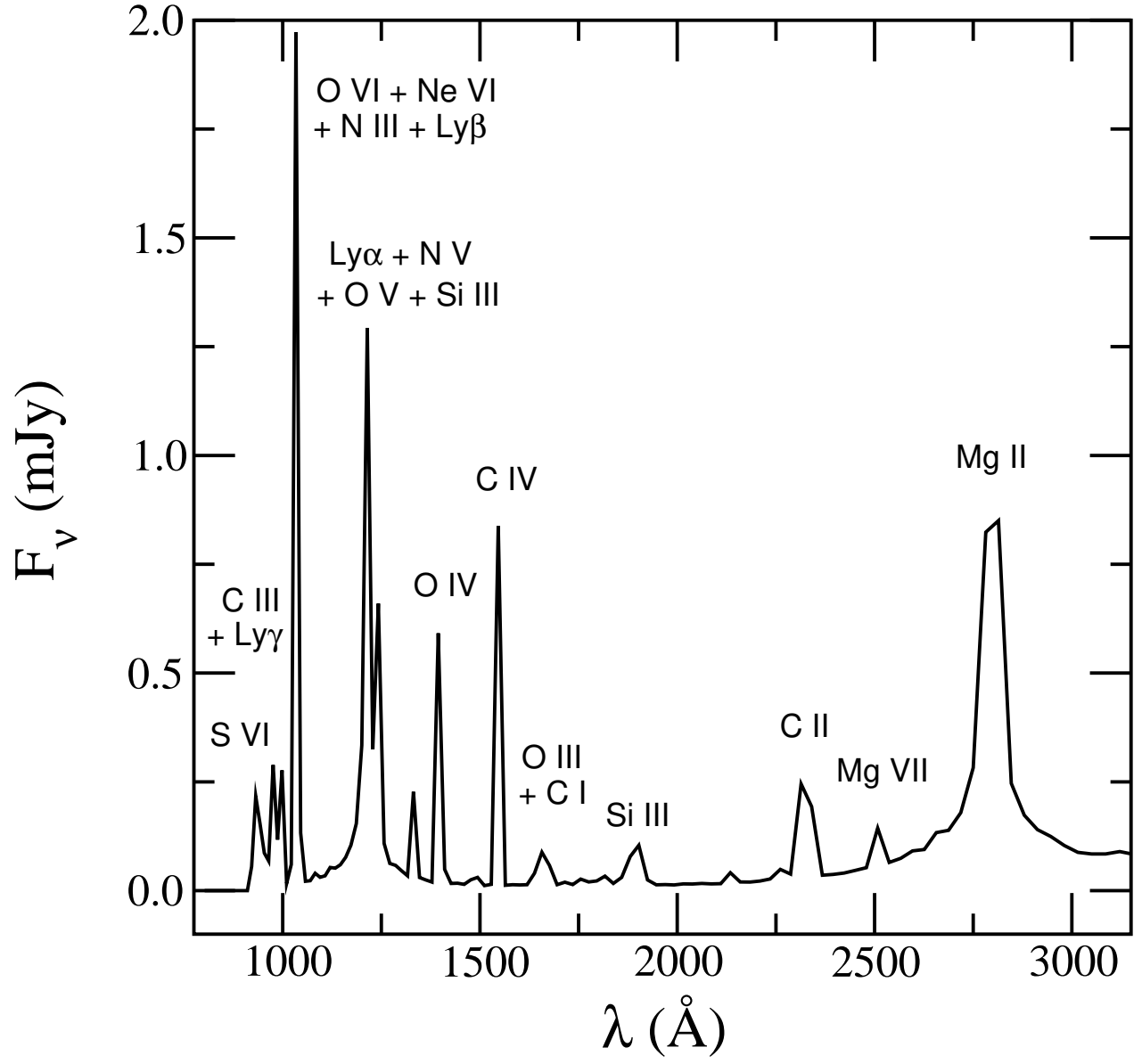


Fig. 6. | Modeled ultraviolet spectrum .

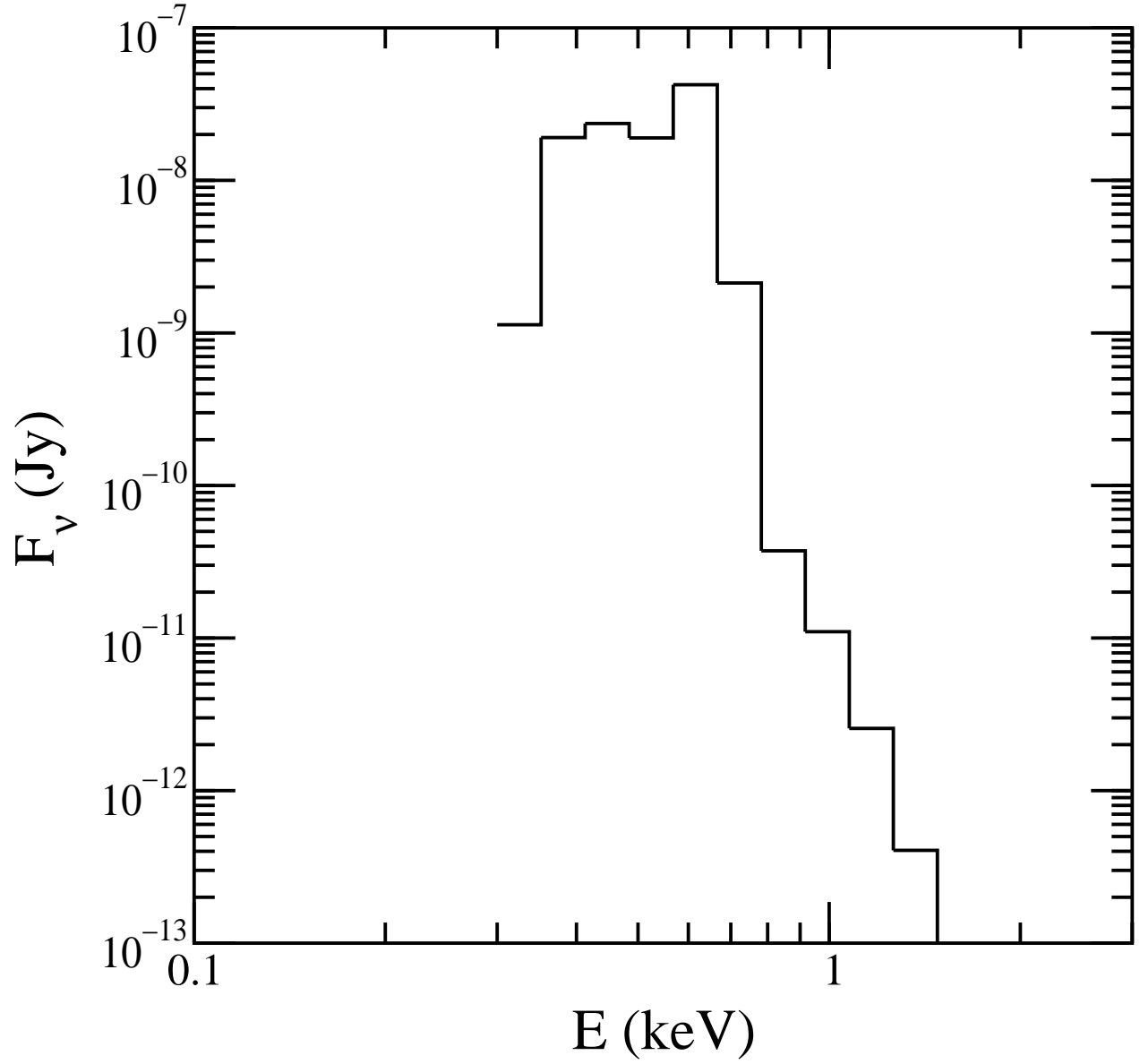


Fig. 7. | Modeled X-ray spectrum, rebinned in equal logarithmic intervals.

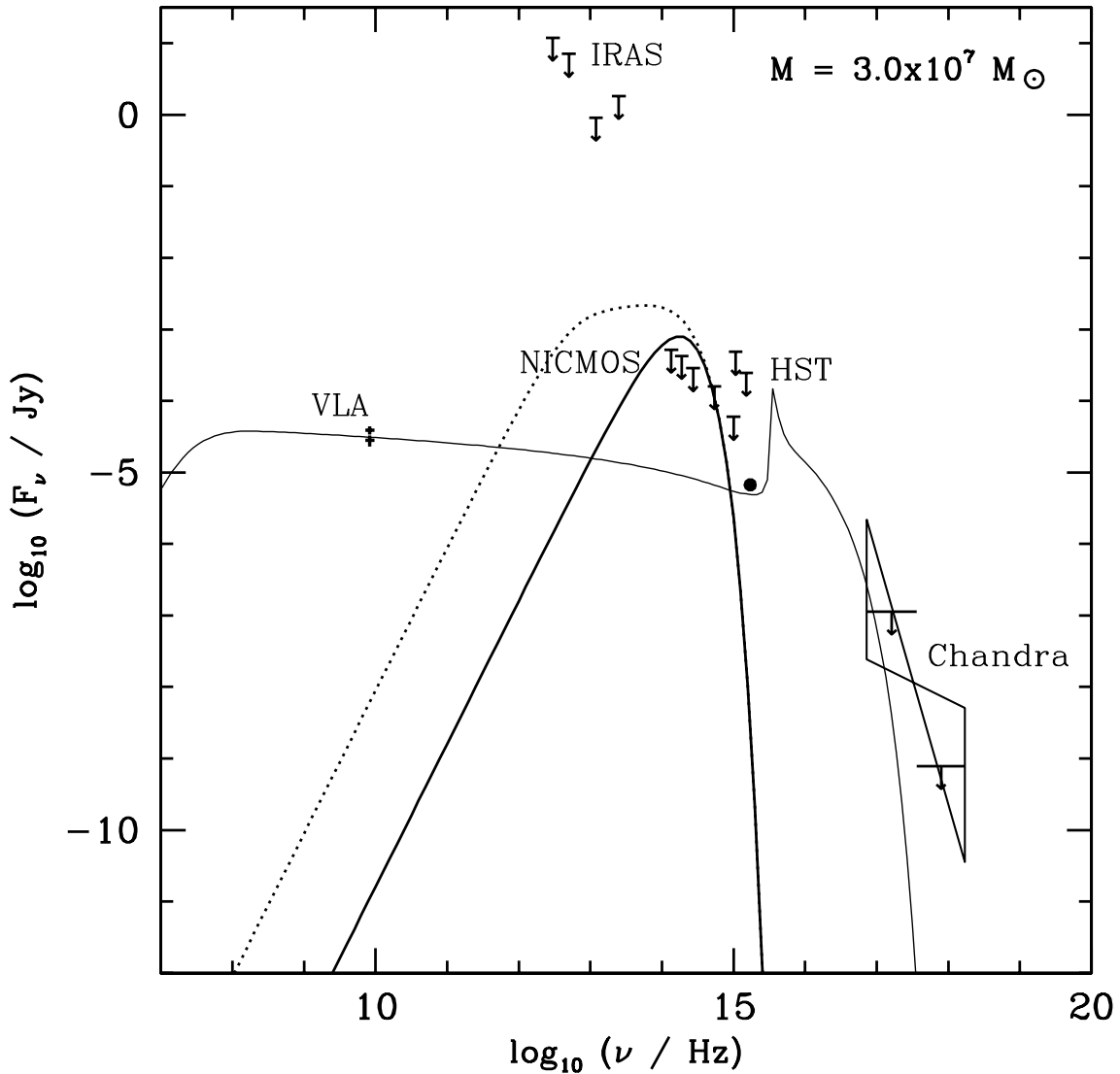


Fig. 8. Spectra of optically thick disks. The disks have an inclination angle of 60° , an inner boundary of $3r_s$ and the accretion rate is $5.0 \times 10^8 \text{ g s}^{-1}$. The thick solid line corresponds to a small disk with an outer boundary of $10r_s$, while the dotted line corresponds to a disk with an outer boundary of $1000r_s$. The thin solid line corresponds to the best-fit radial accretion model, though here only the hydrogen line emission is included. As in Fig. 3, the X-ray upper limits correspond to the so-called "southern" source detected near M 31* by Chandra, whereas the butterfly shows the measured spectrum for the "northern" source. In this best-fit, we have treated these X-ray data as upper limits to the actual spectrum of M 31* (see text).